

Seeing Through The Noisy Dark: Toward Real-world Low-Light Image Enhancement and Denoising

Jiahuan Ren^{1,2}, Zhao Zhang^{1,2,*}, Richang Hong^{1,2}, Mingliang Xu³, Yi Yang⁴, and Shuicheng Yan⁵

¹School of Computer Science and Information Engineering, Hefei University of Technology, Hefei 230009, China

²Key Laboratory of Knowledge Engineering with Big Data (Ministry of Education) & Intelligent Interconnected Systems Laboratory of Anhui Province, Hefei University of Technology, Hefei 230009, China

³School of Information Engineering, Zhengzhou University, Zhengzhou, China

⁴School of Computer Science and Technology, Zhejiang University, Hangzhou, China

⁵Sea AI Lab (SAIL), Singapore

* Corresponding author E-mail: cszzhang@gmail.com

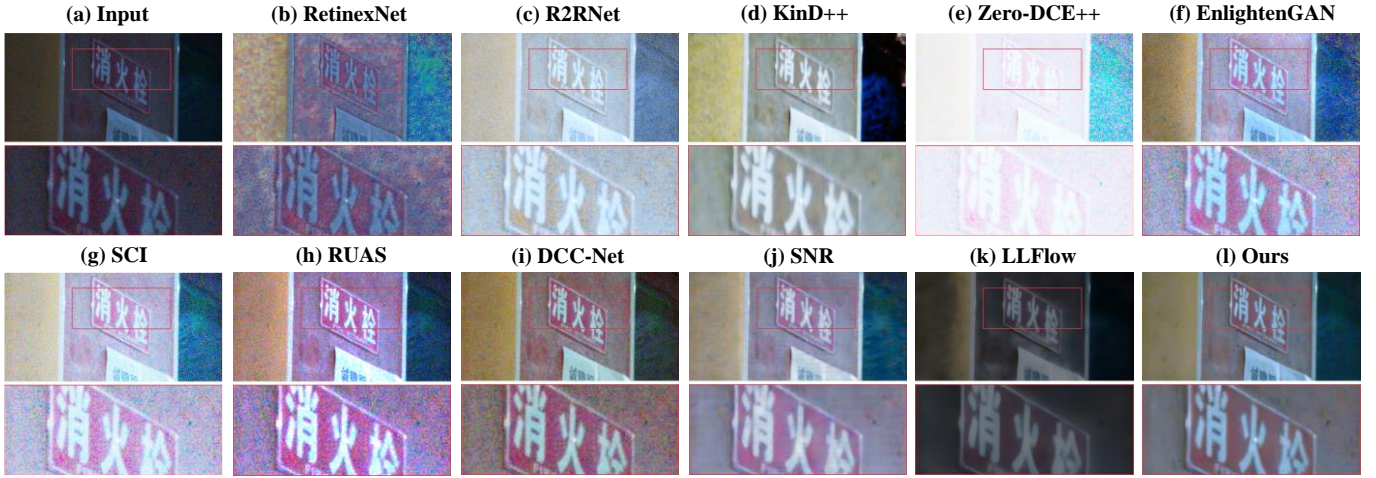


Fig. 1: LLIE comparison based on a real-world image taken in the noisy dark. Clearly, our RLED-Net can effectively see through the noisy dark, while removing the noise and preserve more details. In contrast, the enhanced images of other compared methods (b-k) still contain some speckle noise and blur.

Abstract—Images collected in real-world low-light environment usually suffer from lower visibility and heavier noise, due to the insufficient light or hardware limitation. While existing low-light image enhancement (LLIE) methods basically ignored the noise interference, and mainly focus on refining the illumination of the low-light images based on benchmarked noise-negligible datasets. Such operations will make them inept for the real-world LLIE (RLLIE) task with noise, and result in speckle noise and blur in the enhanced images. Although several LLIE methods considered the noise in low-light image, they are trained on the raw data and hence cannot be directly used for sRGB images, since the domains of data are different, and lack of expertise or unknown protocols. In this paper, we clearly consider the task of seeing through the noisy dark in sRGB color space, and propose a novel end-to-end method termed *Real-world Low-light Enhancement & Denoising Network* (RLED-Net). Since images can usually be characterized by low-rank subspaces in which the redundant information and noise can be removed, we design a *Latent Subspace Reconstruction Block* (LSRB) for feature extraction and denoising. To reduce the loss of global features (color/shape information) and extract more accurate local features (edge/textture information), we also present a basic layer with two parallel branches, called *Cross-channel & Shift-window Transformer* (CST). Based on CST layers, we further present a new backbone to design a U-structure Network (CSTNet) for deep feature recovery, and also design a *Feature Refine Block* (FRB) to refine the final features. Extensive experiments on real noisy images and public databases verified the effectiveness of our RLED-Net for both RLLIE and denoising.

Keywords— Real-world low-light image enhancement and denoising, local and global feature coding; deep feature recovery; seeing through the noisy dark.

I. INTRODUCTION

Low-light image enhancement (LLIE) has been playing important roles in different vision tasks in low-light environment suffering from poor visibility, e.g., detecting, recognizing and segmenting objects in the dark [1-11]. LLIE aims to obtain the norm-light images by estimating the illumination of low-light images to enhance the perception of the low-light images.

Traditional LLIE methods often enhance the illumination of low-light images by designing minimal reconstruction models, e.g., Retinex-based [4] and histogram equalization-based ones. However, they usually cannot restore the detailed information, due to the limited learning ability. Recently, based on the strong fitting ability of deep learning, deep LLIE networks have been proposed, such as Retinex based networks [2-4, 7-11] and the end-to-end deep learning models [5-6, 12-17, 36-38]. However, these methods focus on refining the illumination of images via benchmarked noise-negligible datasets, while neglecting noise interference will enable them to be incapable of handling the RLLIE task well, as can be seen from the results on real-world noisy dark image in Fig.1. Therefore, we ask: *What decreases the performance of deep LLIE methods on real noisy low-light*

images? We attempt to answer this question from three aspects:

(1) Noise negligible assumption. Most current deep LLIE methods tended to only consider the brightness and visibility of the image itself, while did not take into account that all images captured at night have varying degrees of noise. That is, current models mainly consider the image captured in an “ideal” condition and the deep models are usually trained on benchmarked noise-negligible datasets. However, due to the involvement of noise in the real low-light images obtained in the noisy dark, current deep LLIE methods will cause inaccurate restorations (e.g., speckle noise and blur), as can be seen in Fig.1.

(2) Unreasonable consistency assumption. The basic idea of RetinexNet based methods [2-4, 7-11] is that low-light images depend on reflectance and illumination, and assumes that the reflectance of low-light and normal-light images should be the same (i.e., reflectance consistency), and the brightness of the image only depends on the illumination. However, when the low-light images contain noise, RetinexNet assumes the noise only exists in reflectance, while the reflectance of normal-light image is noise-free. In other words, RetinexNet based methods violate the reflectance consistency. In addition, we find that due to the inaccurate decomposition as shown in Fig.2, noise exists in both reflectance and illumination, which makes the supervised information inaccurate and detrimental to enhancement.

(3) Raw data dependent. A few end-to-end deep methods have considered the noise in the process of LLIE [36-39], but they are usually trained on linear raw data and cannot be used for non-linear sRGB image [40], since the domains of data are different and lack of expertise or unknown protocols. Compared with the raw data containing less noise, which are usually unavailable, sRGB is the most widely used color space and the images in sRGB color space usually consist of more noise. In other words, the joint task of denoising and enhancement in sRGB color space will be more difficult than raw data.

To address the aforementioned issues in LLIE, the authors of [41] proposed to remove the noise in low-frequency layer and enhance the details in high-frequency layer, however the noise is also inevitable in high-frequency domain and will be unpredictably amplified during the process of LLIE. Therefore, we present a new end-to-end network for seeing through the noisy dark, which towards real-world LLIE and denoising in sRGB color space. The main contributions are summarized as follows:

(1) RLED-Net: toward seeing through the noisy dark. Technically, we propose a new end-to-end real-world low-light image enhancement & denoising network termed RLED-Net to improve the visibility of noisy low-light images in sRGB color space. This setting can effectively avoid the inaccurate representations caused by the unreasonable consistency assumption in RetinexNet and can make the trained model more suitable for real noisy dark scene. The whole framework of our RLED-Net is shown in Fig.3, and it includes three main components, i.e., a *Latent Subspace Reconstruction Block* (LSRB) for the shallow feature extraction and denoising, a network CSTNet based on the designed basic *Cross-channel & Shift-window Transformer* (CST) layers for feature reconstruction, and a *Feature Refine Block* (FRB) for final feature refining.

(2) Feature representation with noise suppression. Real noise is usually complex and hard to be separated in layers. To enable our model to generalize well to real-world images,

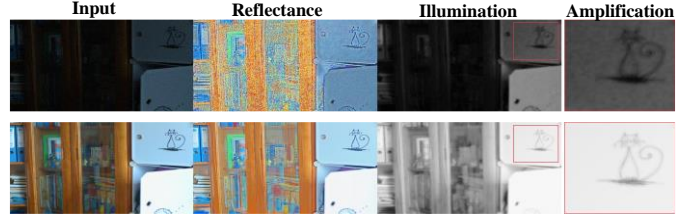


Fig. 2: Decomposition process of RetinexNet, where first and second rows denote the low-light and normal-light images, respectively. It is clear from the amplification that the illumination of low-light image contains noise.

instead of removing noise on the layers or evaluating the noise maps, we aim to suppress the noise by representing image data by low-rank subspaces. Specifically, LSRB is designed to extract features, retain the low-rank structures and suppress noise. Besides, limited information are provided by low-light images and the included noise usually result in failure of restoring the global color and shape information, as well as local edge and texture information. Therefore, we propose the basic layer CST to capture more useful information to improve the RLLIE task.

(3) SOTA performance on both synthetic and real noisy images. Extensive simulations on benchmark low-light image databases with/without noise verified the effectiveness of our model for LLIE and denoising. To test the generalization ability of our RLED-Net to the real-world low-light images, we also collect noisy low-light images from real-world environment for evaluations and better visual results are still obtained.

II. RELATED WORKS

A. End-to-End LLIE Networks

The networks of this kind output the enhanced results directly from the input low-light images [45]. Based on whether paired data are used for training, current methods can be divided into supervised and unsupervised modes [46].

Supervised methods. LLNet [15] is the first network with deep architecture for image enhancement. For the strong ability of convolution, lots of CNN based models have been proposed [5-6, 12-17]. To fully use the edge detailed information, a deep hybrid network [12] is proposed, which includes content and edge streams to simultaneously learn global content and salient structure of sharp images in a unified network. DCC-Net [5] handles the LLIE task by decomposing the color images into gray images and color histogram, so that the color consistency between the enhanced image and ground-truth can be preserved. SNR [6] handles the LLIE task by collectively exploiting long and short range operations with Signal-to-Noise Ratio (SNR) prior to dynamically enhance the pixels with spatial-varying operations. LLFlow [42] proposes a normalizing flow network to take low-light images/features as the condition and maps the distribution of normal-light images to model the conditional distribution. The network proposed by [41] remove the noise in low-frequency layer and enhances the details in high-frequency layer. It should be noted that the necessity of paired images for training will directly limit their real-world applications.

Unsupervised methods. More recently, some unsupervised LLIE methods are proposed. For example, EnlightenGAN [19] designs a dual-discriminator to balance the global and local low-light enhancement, and a self-regularized perceptual loss to constrain the distance between the low-light and enhanced

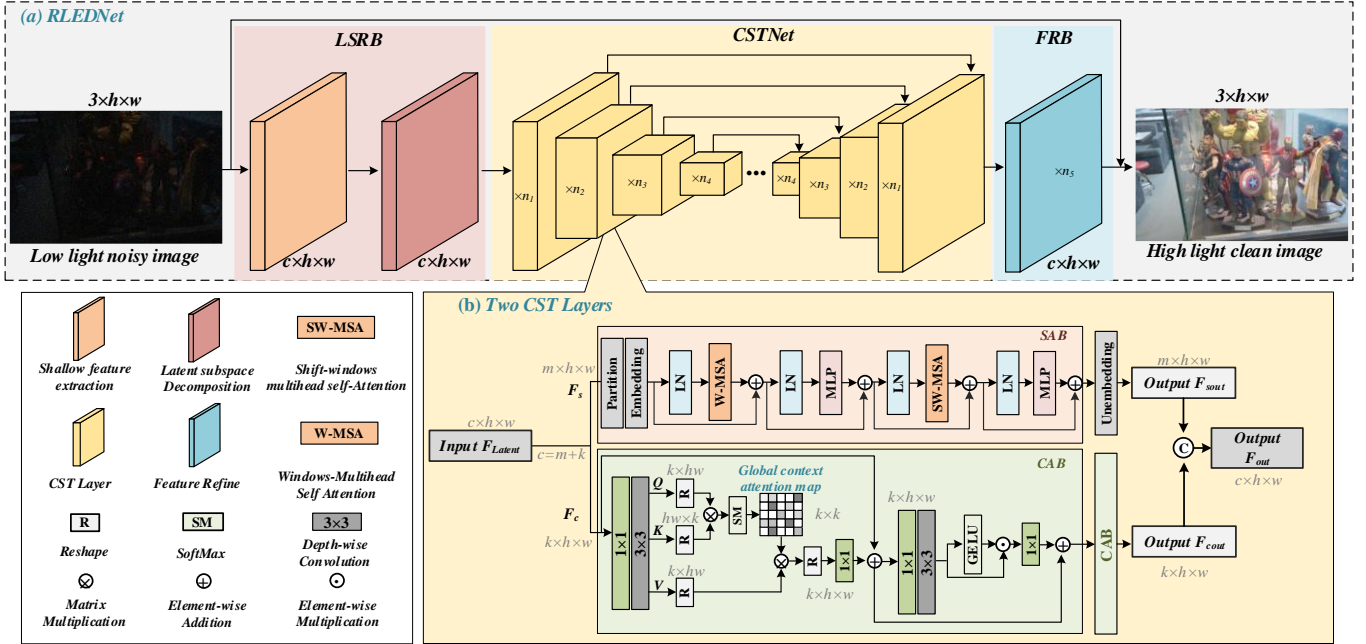


Fig. 3: The framework of our RLED-Net (a), which consists of three parts: *Latent Subspace Reconstruction Block* (LSRB), *CST based Network* (CSTNet) and *Feature Refine Block* (FRB). Each encoder and decoder of CSTNet include multiple CST layers, and the structure of two CST layers is shown in (b).

images. ZeroDCE++ [17] formulates the LLIE task as an image-specific curve estimation problem using a deep network. SCI [35] proposes a lightweight cascaded illumination learning process with weight sharing to handle the LLIE task.

Although these deep models may remove noise to some extent due to the end-to-end learning manner, they mainly consider the problem of LLIE, without considering the unavoidable noise problem explicitly in the real dark environment. Although [41] considered the noise in low-frequency layer, the noise is inevitable in the high-frequency layer and will be unpredictably amplified during the process of image enhancement.

B. Retinex based Networks for LLIE

The basic theory of Retinex [4] is that the color of the objects in image is not affected by the non-uniform light, and the reflectance of the low-light and normal-light images are the same (i.e., color consistency). Specifically, RetinexNet decomposes the images into reflectance and illumination as follows:

$$S = R \circ I, \quad (1)$$

where S is the observed image, R and I are the corresponding reflectance and illumination. \circ is the pixel-wise product. Note that traditional Retinex methods treat the recovered reflectance R as the enhanced result. While the RetinexNet based methods [1, 3, 7-11, 16, 34] usually train a *Decomposition-Net* to obtain the reflectance R and illumination I , which needs low-light and normal-light images to provide supervised prior for low-light images. Let R_{low} and I_{low} denote the reflectance and illumination of low-light images S_{low} respectively, and let R_{normal} and I_{normal} denote the reflectance and illumination of normal-light images S_{normal} respectively. The *Decomposition-Net* usually adopts the following reconstruction loss L_{recon} :

$$L_{recon} = \sum_{i=low, normal} \sum_{j=low, normal} \|R_i \circ I_j - S_j\|_1. \quad (2)$$

Then, the *Reflectance Restoration-Net* is trained based on the

obtained R_{low} and R_{normal} , which also can be regarded as a denoising network. An invariable loss L_{ir} is used to constrain the reflectance consistency of low-light and normal-light images:

$$L_{ir} = \|R_{low} - R_{normal}\|_1. \quad (3)$$

The *Illumination Adjustment-Net* is usually trained based on the decomposed reflectance R_{low} , R_{normal} and illumination I_{low} , I_{normal} with different elaborate losses. Finally, the enhanced results are obtained by $S = R \circ I$. For the noise in images, they assume that the noise only exist in reflectance R_{low} and employ an existing denoising network to R_{low} or treat *Reflectance Restoration-Net* as a denoising network.

Comment: Noise is unavoidable for real-world dark images and aforementioned losses, especially L_{recon} , will be incapable of decomposing images well. First, the reflectance consistency between low-light and normal-light images is not satisfied, i.e., the reconstructed representations $R_{low} \circ I_{normal}$ and $R_{normal} \circ I_{low}$ cannot approximate S_{normal} and S_{low} , respectively. This will result in inaccurate decompositions. Second, the obtained illumination also contains noise, as shown in Fig.2, which will make the recovered images still contain noise. Third, each sub-network is trained individually, which lacks of interaction and will result in a gap between the components and the restored images.

III. PROPOSED METHOD

RLED-Net is mainly proposed to improve the visibility of the real-world low-light images by seeing through the noisy dark, whose framework is shown in Fig.3. Clearly, it contains three main components, i.e., LSRB, CSTNet and FRB. Real-world low-light images usually not only include low-resolution pixels, but also unavoidable noise, while these usually would be inevitably amplified during the process of LLIE, and hence resulting in speckle noise and blur. LSRB is thus proposed to characterize the dark images using low-rank subspaces to suppress the noise, which can effectively reduce the influence of noise.

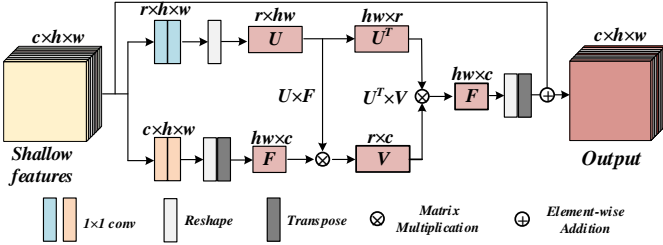


Fig. 4: The process of latent subspace decomposition.

The low-resolution pixels and disturbing noise will also result in losing the details and producing larger chromatic aberration. To obtain more accurate global and local features, CST layer is proposed, and we design a CSTNet and an FRB stage for deep feature extraction and refining. In what follows, we introduce the details of our RLED-Net according to the sequence of data flow to make the procedures easier to understand.

A. Overall Pipeline and Loss

Given a noisy low-light color image $X \in \mathbb{R}^{3 \times h \times w}$, where c , h and w are the number of channels, height and width respectively, RLED-Net firstly feeds it into LSRB to obtain latent features $F_{LSRB} \in \mathbb{R}^{c \times h \times w}$ and suppresses the noise to some extent, which can therefore avoid blurs. Then, F_{LSRB} are sent into CSTNet to obtain deep features $F_{CSTNet} \in \mathbb{R}^{2 \times c \times h \times w}$, where CSTNet includes four encoder-decoder pairs, and each pair consists of multiple CST layers. After that, F_{CSTNet} is passed to FRB and is mapped into the same dimension as the original low-light image to get a residual image $F_{FRB} \in \mathbb{R}^{3 \times h \times w}$. Finally, the restored image Y can be obtained as $Y = X + F_{FRB}$. The loss function contains three parts, i.e., l_1 -loss (l_1), $ssim$ loss (l_{ssim}) and TV loss (l_v):

$$L_{total} = l_1(Y, Y) + l_{ssim}(Y, Y) + \lambda l_v(Y), \quad (4)$$

where Y denotes the predicted result and Y is the ground-truth. Losses l_1 , l_{ssim} and l_v are respectively formulated as

$$\begin{aligned} l_1(Y, Y) &= \|Y - Y\|_1 \\ l_{ssim}(Y, Y) &= 1 - \left(\frac{2\mu_X\mu_Y + c_1}{\mu_X^2 + \mu_Y^2 + c_1} \cdot \frac{2\sigma_{XY} + c_2}{\sigma_X^2 + \sigma_Y^2 + c_2} \right), \\ l_v(Y) &= \sum_{i,j} \left[(Y_{i,j-1} - Y_{i,j})^2 + (Y_{i+1,j} - Y_{i,j})^2 \right] \end{aligned} \quad (5)$$

where μ_X, μ_Y and σ_X, σ_Y denote the mean values and variances of the images X and Y to prevent the denominator from being zero, and λ is a trade-off parameter.

B. Latent Subspace Reconstruction Block (LSRB)

We design LSRB for latent feature extraction, by avoiding the speckle noise or blur in the process of LLIE. Images can usually be represented by low-rank structures [20-24, 43] and the low-rank optimization problem is usually solved by ALM [25] or ADMM [26] that is time-consuming and non-differentiable. Inspired by [24], the plug-and-play and differentiable LSRB is designed. Specifically, LSRB contains a 3×3 convolution for shallow feature extraction and a latent subspace decomposition for feature denoising. As shown in Fig.4, several convolutions are used to generate two low-rank matrices: coefficient matrix U and basis matrix V . Specifically, the original low-light image

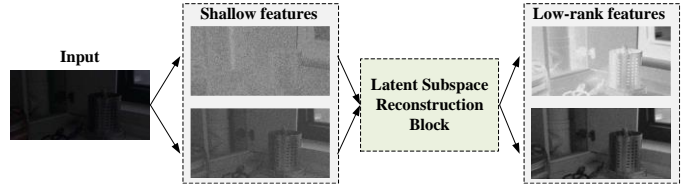


Fig. 5: The denoising process via low-rank decomposition, where LSRB learns two low-rank matrices by matrix factorization based on shallow features, and then reconstructs the features to remove the included noise.

$X \in \mathbb{R}^{3 \times h \times w}$ is firstly fed into a feature extraction module:

$$F_{shallow} = f_{3 \times 3}(X) \in \mathbb{R}^{c \times h \times w}, \quad (6)$$

where $f_{3 \times 3}(\cdot)$ is 3×3 convolution. Then, shallow features $F_{shallow}$ are applied to learn low-rank matrices to approximate $F_{shallow}$ by feeding them to the latent subspace decomposition to obtain the lowest-rank representation. A series of 1×1 convolutions are used for learning the matrixes U and V . As shown in Fig.4, the process of learning the coefficient matrix U is defined as

$$\begin{aligned} F_U &= GELU\left(f_{1 \times 1}\left(GELU\left(f_{1 \times 1}(F_{shallow})\right)\right)\right) \in \mathbb{R}^{r \times h \times w} \\ U &= \text{Reshape}(F_U) \in \mathbb{R}^{r \times hw} \end{aligned}, \quad (7)$$

where $f_{1 \times 1}(\cdot)$ is a 1×1 convolution, $GELU(\cdot)$ is an activation function [27], $\text{Reshape}(\cdot)$ is a flatten operation to convert a 3D matrix to a 2D matrix, and r is the rank of matrix. The process of learning the basis matrix V is formulated as

$$\begin{aligned} F_V &= GELU\left(f_{1 \times 1}\left(GELU\left(f_{1 \times 1}(F_{shallow})\right)\right)\right) \in \mathbb{R}^{c \times h \times w} \\ F &= \text{Trans}(\text{Reshape}(F_V)) \in \mathbb{R}^{hw \times c} \\ V &= U \times F \in \mathbb{R}^{r \times c} \end{aligned}, \quad (8)$$

where $\text{Trans}(\cdot)$ is transpose operation. The basis V can also be regarded as the low-rank representation with dimension being r , where $r \ll hw$. Finally, we can obtain the denoised feature as

$$\begin{aligned} F &= U^T \times V \in \mathbb{R}^{hw \times c} \\ F_{LSRB} &= \text{Trans}(\text{Reshape}^T(F)) \in \mathbb{R}^{c \times h \times w}, \end{aligned}, \quad (9)$$

where $\text{Reshape}^T(\cdot)$ is used to convert a 2D matrix back to a 3D matrix. Then, the obtained denoised features F_{LSRB} are transferred into CSTNet, which can also suppress the impact of the noise on the restoration process to a certain extent. The reconstructed features are illustrated in Fig.5.

C. CST based Network (CSTNet)

The low-resolution pixels of low-light images will pose greater challenges and cannot provide sufficient useful information to recover the detailed information and brightness. A basic feature extraction layer (CST) with two parallel branches is therefore proposed. CST layer has a *Shifted-windows Attention Branch* (SAB) for local feature extraction, and a *Crossed-channel Attention Branch* (CAB) to learn global information. Although SAB can extract local features, it needs to mask some windows to make the calculation of self-attention occurs between windows with the same index. However, such operations and shift strategy will result in limited self-attention calculation for the windows located at the image boundary and cause insufficient interaction between windows, which will lose important global

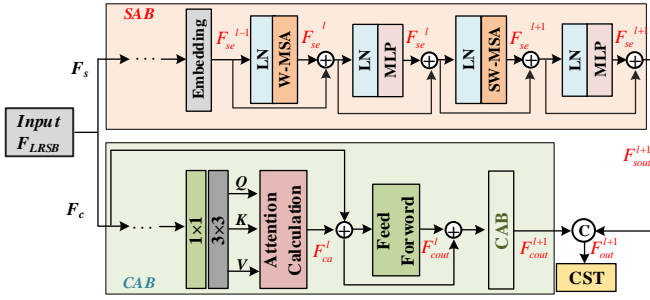


Fig. 6: The detailed feature calculation process in CST.

information [28, 29]. As such, we design the convolution based branch CAB. Similar to [18], CAB calculates the self-attention on the crossed channels by the Multi-Head Attention [30] to the image restoration task to obtain crossed-channels global context, which will be beneficial for modeling the long-distance dependency. The schematic diagram of CST is shown in Fig.3 (b). We stack multiple CST layers to form four encoders and decoders to construct CSTNet. In this study, the number n_i of the CST layers in each encoder/decoder is set to four.

For the features $F_{LSRB} \in \mathbb{R}^{c \times h \times w}$, CST divides them into two parts: $F_s \in \mathbb{R}^{m \times h \times w}$ and $F_c \in \mathbb{R}^{k \times h \times w}$, where $m+k=c$. SAB firstly partitions F_s into many windows (tokens) and then flattens them by linear embedding, denoted as F_{se} . Then, the process of calculating the windows based self-attention is defined as

$$\begin{aligned} F_{se}^l &= W_MSA \left[LN \left(F_{se}^{l-1} \right) \right] + F_{se}^{l-1} \\ F_{se}^l &= MLP \left[LN \left(F_{se}^l \right) \right] + F_{se}^l \\ F_{se}^{l+1} &= SW_MSA \left[LN \left(F_{se}^l \right) \right] + F_{se}^l, \\ F_{se}^{l+1} &= MLP \left[LN \left(F_{se}^{l+1} \right) \right] + F_{se}^{l+1} \end{aligned} \quad (10)$$

where MLP and LN denote the Multilayer Perceptron [30] and LayerNorm [31], respectively. W_MSA and SW_MSA denote the window based multi-head self-attention and shifted window partitioning configurations, respectively. l denotes the l -th layer in the windows self-attention. F_{se}^l and F_{se}^l denote the features of W_MSA and MLP in the l -th layer, respectively. F_{se}^0 denotes the embedding features. Finally, the features of the last layer $F_{se}^{n_i}$ will be transformed into the same dimension as that of the original input features, denoted as $F_{sout} \in \mathbb{R}^{m \times h \times w}$.

For CAB, the features F_c are fed into a 1×1 convolution for the pixel-wise aggregation of crossed-channel context and also a 3×3 depth-wise convolution for encoding channel-wise spatial context. Based on the enriched context, the terms *Query* (Q), *Key* (K) and *Value* (V) can be obtained as

$$\begin{aligned} Q, K, V &= f_{3 \times 3}^d \left(f_{1 \times 1} \left(F_c \right) \right) \\ Q &\in \mathbb{R}^{k \times h \times w}, K \in \mathbb{R}^{k \times h \times w}, V \in \mathbb{R}^{k \times h \times w}. \end{aligned} \quad (11)$$

Then, Q , K and V will be reshaped to $Q \in \mathbb{R}^{k \times h \times w}$, $K \in \mathbb{R}^{h \times w \times k}$ and $V \in \mathbb{R}^{k \times h \times w}$, respectively. Q and K are employed to generate the crossed-channels global context attention map $G \in \mathbb{R}^{k \times k}$ by dot product. Then, the crossed-channel attention based features F_{ca} in the l -th layer can be calculated by the following formula:

$$\begin{aligned} CA(Q, K, V) &= \text{Softmax}(Q \cdot K / \alpha) \cdot V \\ F_{ca}^l &= f_{3 \times 3}^d \left(CA(Q, K, V) \right) + F_c \end{aligned} \quad (12)$$

Finally, a feed-forward network [18] is applied for the final output of CAB by Eq. (13) to transform the features F_{ca} . That is, it uses the depth-wise convolution for learning the local structures of images for effective restoration:

$$\begin{aligned} F_{fd} &= f_{3 \times 3}^d \left(f_{1 \times 1} \left(LN \left(F_{ca} \right) \right) \right) \\ F_{cout}^l &= GELU \left(F_{fd} \right) \odot F_{fd} + F_{ca} \end{aligned} \quad (13)$$

After both $F_{sout} \in \mathbb{R}^{m \times h \times w}$ and $F_{cout} \in \mathbb{R}^{k \times h \times w}$ are calculated, the output features F_{CSTNet} of the CST layer can be obtained by concatenating the features F_{sout} and F_{cout} . The detailed feature calculation process in the CST layer is exhibited in Fig.6.

D. Feature Refine Block (FRB)

After the reconstructed features are obtained, we feed them into the FRB and calculate the final recovered images by generating a residual image F_r , where FRB is also stacked by several CST layers and a 3×3 convolution. The process is formulated as

$$F_r = f_{3 \times 3} \left(\underbrace{CST \left(\dots CST \left(F_{out} \right) \right)}_{n_5} \right) \in \mathbb{R}^{3 \times h \times w}, \quad (14)$$

$$Y = X + F_r,$$

where n_5 is the number of CST layers, $F_r \in \mathbb{R}^{3 \times h \times w}$ is the residual image and Y denotes the restored image.

IV. EXPERIMENTAL RESULTS AND ANALYSIS

We mainly evaluate our RLED-Net for noisy low-light image enhancement. In this study, ten closely-related popular deep LLIE methods are included for comparison, including RetinexNet [3], R2RNet [32], KinD++ [7], ZeroDCE++ [16], EnlightenGAN [19], RUAS [34], SCI [35], SNR [6], DCC-Net [5] and LLFlow [42]. Three benchmarked datasets, i.e., LOL [3], LSRW [32] and RELLISUR [33], and some real-world images taken by mobile devices at night are employed for evaluations. For our RLED-Net, the number of CST layers in each encoder-decoder and FRB is set to 4. The learning rate is 0.0001 and the trade-off parameter $\lambda = 0.1$. The rank r in the LSRB is set to 8. For performance comparison and evaluations, 4 widely-used metrics, i.e., peak signal-to-noise ratio (PSNR), structural similarity (SSIM) mean absolute error (MAE) and Color-Sensitive Error (CSE) [44] are applied. Different from the PSNR, SSIM and MAE metrics, CSE is a chromatic aberration evaluation metric that can directly measure the color difference between a pair of images. Similar to MAE, the smaller the CSE value, the better the enhancement result. All the experiments are carried out and compared a PC with two 2080Ti GPUs.

A. Evaluation on RELLISUR Dataset

We first evaluate each method on the RELLISUR dataset [33] that consists of both in-door and outdoor scenes captured by a DSLR camera. RELLISUR has 850 low-light/normal-light image pairs and each low-light image corresponds to five under-exposed images. In this study, we adopt the low-light images with exposure value being -3.5 for training and testing. To verify the enhancement and denoising ability, Gaussian noise with noise level $\sigma = 10$ is added to the low-light images. The quantitative results are described in Table 1, and some visual results of enhanced images are exhibited in Fig.7. We find that: 1) compared with the other methods, our RLED-Net achieves

Table 1: The quantitative results in terms of PSNR, SSIM, CSE (10^3) and MAE (%) of all competing methods on the noisy RELLISUR and LSRW datasets ($\sigma=10$), where the **bold** denotes the best.

Datasets		Methods										
		RetinexNet	R2RNet	KinD++	ZeroDCE++	RUAS	SCI	EnlightenGAN	DCC-Net	SNR	LLFlow	Ours
RELLISUR	PSNR	17.02	19.82	19.05	8.79	10.47	11.69	12.29	21.75	21.73	21.62	22.48
	SSIM	0.28	0.66	0.69	0.05	0.08	0.08	0.10	0.75	0.72	0.71	0.77
	CSE	18.08	28.00	27.81	145.21	152.65	148.92	53.67	22.66	8.48	19.07	5.71
	MAE	11.70	8.61	9.79	30.87	26.25	22.23	20.06	7.03	6.93	6.75	6.48
LSRW	PSNR	16.69	17.24	--	10.03	12.12	13.38	16.09	20.03	20.37	20.21	21.63
	SSIM	0.25	0.58	--	0.07	0.11	0.08	14.63	0.66	0.64	0.66	0.68
	CSE	18.28	15.79	--	80.35	80.20	79.70	34.02	7.94	6.49	4.95	3.94
	MAE	11.99	12.09	--	26.51	21.47	17.99	12.58	7.82	8.38	7.66	7.23



Fig. 7: Visual comparison of the enhanced images (with PSNR/SSIM) based on the RELLISUR dataset.

higher PSNR and SSIM values, and smaller MAE and CSE values than others, followed by DCC-Net, SNR and LLFlow that obtain better results than other remaining methods. That is, RLED-Net can handle the noisy low-light images better and is more robust to noise than other competitors; 2) from the visual results, the enhanced images of other compared methods still contain some speckle noise and blur. While the restored images of our RLED-Net contain less speckle noise and blur. In addition, we see the color of the enhanced images by our method is the closest to that of ground-truth image and the CSE values are lowest, i.e., RLED-Net produce smaller chromatic aberration.

B. Evaluation on LSRW Dataset

We then evaluate each method based on the LSRW dataset [32] that contains 5,650 paired images captured by a Nikon D7500 camera and a HUAWEI P40 Pro mobile phone. We take 2480 paired images taken by Huawei mobile phone for training and 30 paired images for testing. To simulate the real dark night and

evaluate the robustness of each method against noise, Gaussian noise with $\sigma=10$ is also added to the low-light images. The quantitative evaluation results are also shown in **Table 1**, from which similar observations can be obtained. That is, RLED-Net outperforms the other methods for noisy LLIE in terms of four metrics. Similarly, the three recent DCC-Net, SNR and LLFlow methods also obtain highly-competitive results on this dataset.

C. Evaluation on LOL Dataset

We also evaluate each model based on the LOL dataset [3] that contains 485 paired low-light/normal-light images for training and 15 paired images for testing. In this study, we resize all the images into 640×320 for each method. To simulate the real dark night and evaluate the robustness of each method against noise, we add different levels of Gaussian noise ($\sigma=0, 10, 20$) into the low-light images. The quantitative enhancement results are described in **Table 2** and some visual results of the enhanced results with noise level $\sigma=10$ are shown in **Fig.8** as examples.

Table 2: The quantitative results in terms of PSNR, SSIM, CSE (10^3) and MAE (%) of all competing methods on the noisy LOL datasets with different noise levels, where the **bold** denotes the best.

Noise levels		Methods										
		RetinexNet	R2RNet	KinD++	ZeroDCE++	RUAS	SCI	EnlightenGAN	DCC-Net	SNR	LLFlow	Ours
$\sigma=0$	PSNR	16.82	20.20	20.92	16.11	11.32	14.86	18.32	22.15	22.96	24.83	24.38
	SSIM	0.43	0.82	0.80	0.53	0.48	0.61	0.64	0.82	0.86	0.89	0.89
	CSE	6.36	11.66	5.24	24.68	34.43	33.79	10.10	3.78	4.75	2.07	2.14
	MAE	14.93	11.68	8.83	15.89	28.23	19.18	13.71	8.96	7.64	6.59	7.13
$\sigma=10$	PSNR	16.67	18.01	15.16	10.18	10.68	11.98	14.89	15.35	21.72	22.28	22.62
	SSIM	0.35	0.66	0.62	0.10	0.12	0.10	0.23	0.60	0.77	0.78	0.79
	CSE	27.98	32.87	7.12	42.60	44.81	46.13	11.09	17.35	3.41	4.32	2.50
	MAE	12.94	11.58	17.26	26.43	27.85	22.38	15.88	15.18	8.24	7.96	7.25
$\sigma=20$	PSNR	15.04	16.88	16.64	8.30	9.91	10.05	13.21	14.11	20.15	19.29	20.99
	SSIM	0.18	0.64	0.66	0.04	0.05	0.05	0.12	0.49	0.72	0.70	0.74
	CSE	48.27	138.34	8.62	62.58	50.68	52.80	13.89	20.29	2.66	12.41	1.07
	MAE	15.06	12.94	14.92	32.63	28.27	26.47	16.36	16.63	8.46	8.83	8.15

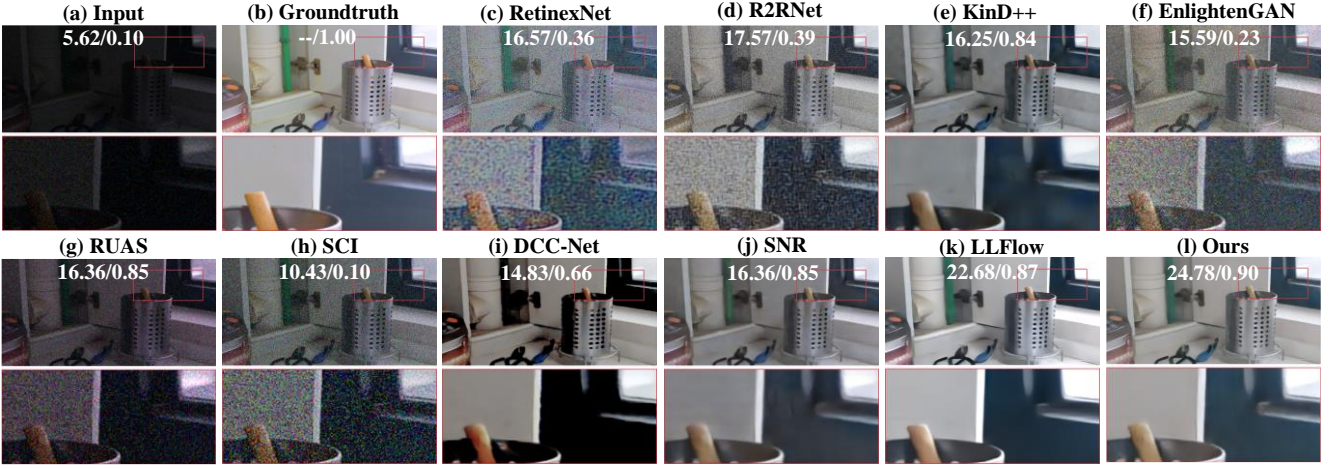


Fig.8: Visual comparison of the enhanced images by each method based on the noisy LOL dataset.

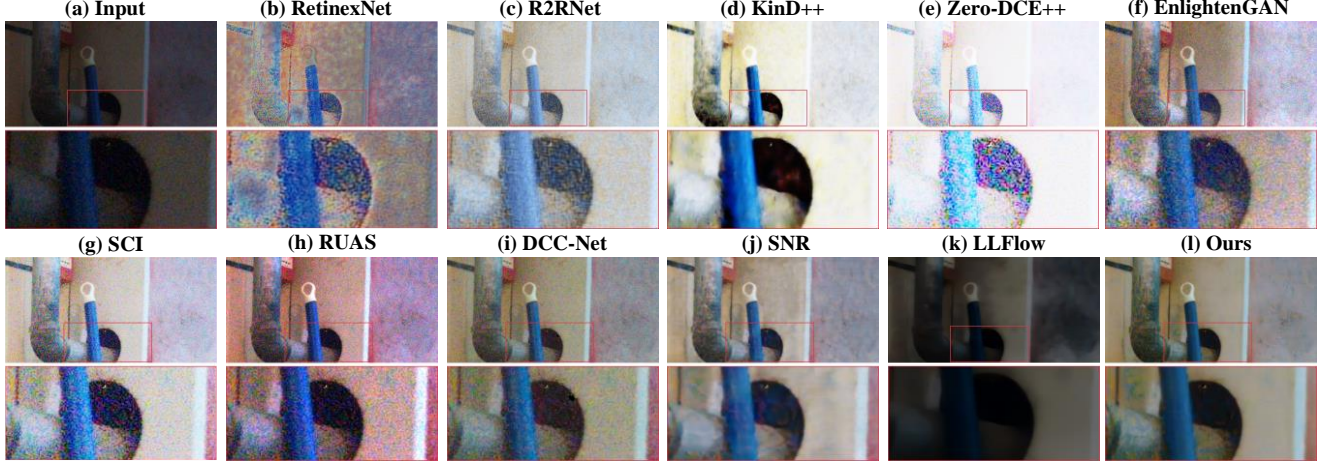


Fig.9: Visual comparison of the enhanced real-world low-light images by each method with real noise.

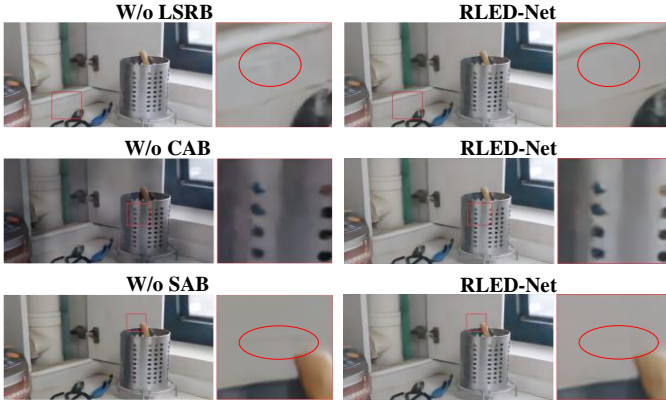
We have the following conclusions. First, from the numerical results in Table 2, we can see that when the original LOL dataset is used, i.e., noise level $\sigma=0$, LLFlow obtains the best result, followed closely by our method. However, when the noise levels increase, the performance of LLFlow drops faster than our RLED-Net, and our method can outperform LLFlow in the noisy cases. Second, from the visualizations in Fig.8, our RLED-Net can remove the noise effectively and obtains better enhancement results. In contrast, almost all other methods have produced blur due to interference of noise in low-light images and still contain much more noise in the recovered images.

D. Evaluation on Real-world Low-Light Images

To evaluate the generalization ability of each deep LLIE model, we also employ some real-world low-light images with noise for LLIE. Due to the lack of paired images for training, we use the model trained on the LOL dataset with Gaussian noise level $\sigma=10$ and test on real low-light images. The visual results are shown in Fig.1 and Fig.9, from which we can observe that our RLED-Net can handle the task better by effectively removing the noise in the real images. More importantly, our method can keep more detail information, which means that our RLED-Net

Table 3: LLIE results of our RLED-Net with different components.

Model	W/o LSRB	W/o SAB	W/o CAB	RLED-Net
PSNR	22.15	22.41	16.91	22.62
SSIM	0.77	0.78	0.72	0.79
MAE (%)	7.98	7.35	15.51	7.25

**Fig. 10:** Visual comparison of different components in our model.

has stronger generalization ability to real cases. In contrast, the enhanced images of other methods contain much more noise and are still blurred due to the influence of noise.

E. Ablation Study

Finally, we evaluate the effect of each component on the performance of our RLED-Net, namely, LSRB, SAB and CAB. To demonstrate the effectiveness of the components in LSRB, we remove the latent subspace decomposition process and reserve the shallow feature extraction. To prove the effectiveness of the components SAB and CAB in CST, we use them separately to build the encoder-decoders and keep the number of channels unchanged. The analysis results are reported in **Table 3**, where **W/o LSRB** denotes RLEDNet without LSRB, **W/o SAB** denotes the encoder-decoders without SAB, and **W/o CAB** denotes the encoder-decoders without CAB. In addition, we also exhibit some visual results in **Fig.10** to show the effectiveness of each component. In this study, noisy LOL dataset with $\sigma=10$ is evaluated. We can conclude that when LSRB is removed, some areas of the restored image are blurred, influenced by the noise; when CAB is removed, the brightness of the restored image becomes uneven, which may be caused by the loss of global information; when we remove SAB, certain local parts become inaccurate. That is, each component will be important for ensuring the performance of our method.

In addition, LSRB module also involves the selection of the rank of low-rank matrix, so we vary the rank of the decomposed matrix from 2 to 32 and the result are reported in **Table 4**, from which we see RLED-Net performs the best as the rank is 8.

Table 4: Comparison on the LOL dataset with varying ranks.

Rank	2	4	8	16	32
PSNR	21.25	21.37	22.62	21.87	20.42
SSIM	0.78	0.78	0.79	0.79	0.78
MAE (%)	7.81	8.09	7.25	7.71	9.03

V. CONCLUDING REMARKS

We explored the challenging task of seeing through the noisy dark in sRGB color space, and proposed an end-to-end method called Real-world Low-light Enhancement & Denoising Net-

work (RLED-Net). To enable our model to be capable of generalizing well to the real-world low-light images with noise, we design a latent subspace reconstruction block by characterizing the low-rank subspace of noisy images, in which the redundant information and noise can be removed. We also design a novel CSTNet with two branches and a simple feature refining block to simultaneously reduce the loss of global color/shape information and local edge/texture information caused by the noise and low-resolution pixel values, and finally refine the features. Extensive experiments show the effectiveness of our model for low-light image enhancement and denoising, and moreover the strong generalization ability to real-world low-light images.

In future, we will explore more effective way to improve the generalization ability for real-world LLIE. In addition, we will discuss more complex LLIE tasks, e.g., low-light environment with extreme non-uniform light or rainy night, in future.

VI. ACKNOWLEDGMENT

This work is partially supported by the National Natural Science Foundation of China (62072151, 61932009, 61822701, 62036010, 72004174), and the Anhui Provincial Natural Science Fund for the Distinguished Young Scholars (2008085J30). Zhao Zhang is the corresponding author of this paper.

REFERENCES

- [1] Chen, Chen, Qifeng Chen, Jia Xu and Vladlen Koltun, “Learning to See in the Dark,” *In: Proceedings of the IEEE/CVF Conference on Computer Vision and Pattern Recognition*, pp.3291-3300, 2018.
- [2] Xiaojie Guo, Li Yu and Ling Haibin, “LIME: Low-Light Image Enhancement via Illumination Map Estimation,” *IEEE Transactions on Image Processing*, vol. 26, pp.982-993, 2017.
- [3] Chen Wei, Wenjing Wang, Wenhan Yang and Jiaying Liu, “Deep Retinex Decomposition for Low-Light Enhancement.” *In: Proceedings of the Proceedings British Machine Vision Conference*, 2018.
- [4] Edwin Herbert Land, “The retinex theory of color vision,” *Scientific American*, vol.237, no.6, pp.108-128, 1977.
- [5] Zhao Zhang, Huan Zheng, Richang Hong, Mingliang Xu, Shuicheng Yan and Meng Wang, “Deep Color Consistent Network for Low-Light Image Enhancement,” *In: Proceedings of the IEEE/CVF Conference on Computer Vision and Pattern Recognition*, 2022.
- [6] Xiaogang Xu, Ruixing Wang, Chiao Fu and Jiaya Jia, “SNR-Aware Low-light Image Enhancement,” *In: Proceedings of the IEEE/CVF Conference on Computer Vision and Pattern Recognition*, 2022.
- [7] Yonghua Zhang, Xiaojie Guo, Jiayi Ma, Wei Liu, Jiawan Zhang, “Beyond Brightening Low-light Images,” *International Journal of Computer Vision*, vol.129, no.4, pp.1013-1037, 2021.
- [8] Wenhan Yang, Wenjing Wang, Haofeng Huang, Shiqi Wang and Jiaying Liu, “Sparse Gradient Regularized Deep Retinex Network for Robust Low-Light Image Enhancement,” *IEEE Transactions on Image Processing*, vol.30, pp.2072-2086, 2021.
- [9] Xutong Ren, Wenhan Yang, Wen-Huang Cheng and Jiaying Liu, “LR3M: Robust Low-Light Enhancement via Low-Rank Regularized Retinex Model,” *IEEE Transactions on Image Processing*, vol.29, pp. 5862-5876, 2020.
- [10] Risheng Liu, Long Ma, Jiaao Zhang, Xin Fan and Zhongxuan Luo, “Retinex-inspired Unrolling with Cooperative Prior Architecture Search for Low-light Image Enhancement,” *In: Proceedings of the IEEE/CVF Conference on Computer Vision and Pattern Recognition*, 2021.
- [11] Wen-Bin Wu, Jian Weng, Pingping Zhang, Xu Wang, Wenhan Yang and Jianmin Jiang, “URetinex-Net: Retinex-Based Deep Unfolding Network for Low-Light Image Enhancement,” *In: Proceedings of the IEEE/CVF Conference on Computer Vision and Pattern Recognition*, 2022.

[12] Wenqi Ren, Sifei Liu, Lin Ma, Qianqian Xu, Xiangyu Xu, Xiaochun Cao, Junping Du and Ming-Hsuan Yang, "Low-Light Image Enhancement via a Deep Hybrid Network." *IEEE Transactions on Image Processing*, vol.28, pp.4364-4375, 2019.

[13] Syed Waqas Zamir, Aditya Arora, Salman Khan, Hayat Munawar, Fahad Shahbaz Khan, Ming-Hsuan Yang and Ling Shao, "Learning Enriched Features for Fast Image Restoration and Enhancement," *IEEE Transactions on Pattern Analysis and Machine Intelligence*, 2022.

[14] Jiaqian Li, Juncheng Li, Faming Fang, Fang Li and Guiyu Zhang, "Luminance-Aware Pyramid Network for Low-Light Image Enhancement," *IEEE Transactions on Multimedia*, vol.23, pp.3153-3165, 2021.

[15] Kin Gwn Lore, Adedotun Akintayo and Soumik Sarkar, "LLNet: A deep autoencoder approach to natural low-light image enhancement," *Pattern Recognition*, vol.61, pp.650-662, 2017.

[16] Chongyi Li, Jichang Guo, Fatih Porikli, and Yanwei Pang, "Lightennet: A convolutional neural network for weakly illuminated image enhancement," *Pattern recognition letters*, vol.104, pp.15-22, 2018.

[17] Chongyi Li, Chunle Guo and Chen Change Loy, "Learning to Enhance Low-Light Image via Zero-Reference Deep Curve Estimation," *IEEE Transactions on Pattern Analysis and Machine Intelligence*, vol.44, pp.4225-4238, 2022.

[18] Syed Waqas Zamir, Aditya Arora, Salman Hameed Khan, Munawar Hayat, Fahad Shahbaz Khan, Ming-Hsuan Yang, "Restormer: Efficient Transformer for High-Resolution Image Restoration," *In: Proceedings of the IEEE/CVF Conference on Computer Vision and Pattern Recognition*, pp. 5718-5729, 2022.

[19] Yifan Jiang, Xinyu Gong, Ding Liu, Yu Cheng, Chen Fang, Xiaohui Shen, Jianchao Yang, Pan Zhou and Zhangyang Wang, "EnlightenGAN: Deep Light Enhancement Without Paired Supervision," *IEEE Transactions on Image Processing*, vol.30, pp.2340-2349, 2021.

[20] Jiahuan Ren, Zhao Zhang, Richang Hong, Mingliang Xu, Haijun Zhang, Mingbo Zhao* and Meng Wang, "Robust Low-Rank Convolution Network for Image Denoising." *In: Proceedings of the ACM International Conference on Multimedia*, Lisbon, Portugal, June 2022.

[21] Zhao Zhang, Jiahuan Ren, Zheng Zhang and Guangcan Liu, "Deep Latent Low-Rank Fusion Network for Progressive Subspace Discovery," *In: Proceedings of the International Joint Conferences on Artificial Intelligence*, Yokohama, Japan, April 2020.

[22] Xu Jun, Zhang Lei, Zhang David, Feng Xiangchu. "Multi-channel weighted nuclear norm minimization for real color image denoising," *In: Proceedings of the IEEE International Conference on Computer Vision*, pp.1096-1104, 2017.

[23] Dong Weisheng, Shi Guangming, Li Xin. "Nonlocal image restoration with bilateral variance estimation: a low-rank approach," *IEEE Transactions on Image Processing*, vol.22, no.2, pp.700-711, 2012.

[24] Hongyan Zhang, Hongyu Chen, Guangyi Yang and Liang-pei Zhang, "LR-Net: Low-Rank Spatial-Spectral Network for Hyperspectral Image Denoising," *IEEE Transactions on Image Processing*, vol.30, pp.8743-8758, 2021.

[25] Zhouchen Lin, Minming Chen and Yi Ma, "The Augmented Lagrange Multiplier Method for Exact Recovery of Corrupted Low-Rank Matrices," *ArXiv abs/1009.5055*, 2010.

[26] Stephen P. Boyd, Neal Parikh, Eric King-wah Chu, Borja Peleato and Jonathan Eckstein, "Distributed Optimization and Statistical Learning via the Alternating Direction Method of Multipliers," *Found. Trends Mach. Learn*, vol.3, no.1, pp.1-122, 2011.

[27] Dan Hendrycks, Kevin Gimpel. "Gaussian Error Linear Units (GELUs)," *arXiv: Learning*, 2016.

[28] Ze Liu, Yutong Lin, Yue Cao, Han Hu, Yixuan Wei, Zheng Zhang, Stephen Lin and Baining Guo, "Swin Transformer: Hierarchical Vision Transformer using Shifted Windows," *In: Proceedings of the IEEE/CVF International Conference on Computer Vision*, pp.9992-10002, 2021.

[29] Jingyun Liang, Jie Cao, Guolei Sun, K. Zhang, Luc Van Gool and Radu Timofte, "SwinIR: Image Restoration Using Swin Transformer," *In: Proceedings of the IEEE/CVF International Conference on Computer Vision Workshops*, pp.1833-1844, 2021.

[30] Ashish Vaswani, Noam M. Shazeer, Niki Parmar, Jakob Uszkoreit, Llion Jones, Aidan N. Gomez, Łukasz Kaiser and Illia Polosukhin, "Attention is All you Need," *In: Proceedings of the 31st Conference on Neural Information Processing Systems, Long Beach, CA, USA*, 2017.

[31] Alexey Dosovitskiy, Lucas Beyer, Alexander Kolesnikov, Dirk Weissenborn, Xiaohua Zhai, Thomas Unterthiner, Mostafa Dehghani, Matthias Minderer, Georg Heigold, Sylvain Gelly, Jakob Uszkoreit and Neil Houlsby, "An image is worth 16x16 words: Transformers for image recognition at scale," *In: Proceedings of the International Conference on Learning Representations*, 2021.

[32] Jiang Hai., Zhu Xuan, Ren Yang, Yutong Hao, Fengzhu Zou, Fang-Ju Lin and Songchen Han, "R2RNet: Low-light Image Enhancement via Real-low to Real-normal Network," *ArXiv abs/2106.14501*, 2021.

[33] A. Aakerberg, K. Nasrollahi and T. B. Moeslund, "RELLISUR: A Real Low-Light Image Super-Resolution Dataset," *In: Thirty-fifth Conference on Neural Information Processing Systems Datasets and Benchmarks Track*, 2021.

[34] Risheng Liu, Long Ma, Jiaao Zhang, Xin Fan and Zhongxuan Luo, "Retinex-inspired Unrolling with Cooperative Prior Architecture Search for Low-light Image Enhancement," *In: Proceedings of the IEEE/CVF Conference on Computer Vision and Pattern Recognition*, pp.10556-10565, 2021.

[35] Long Ma, Tengyu Ma, Risheng Liu, Xin Fan, Zhongxuan Luo, "Toward Fast, Flexible, and Robust Low-Light Image Enhancement." *In: Proceedings of the IEEE/CVF Conference on Computer Vision and Pattern Recognition*, 2022.

[36] Chen Chen, Qifeng Chen, Jia Xu, Vladlen Koltun, "Learning to see in the dark," *In: Proceedings of the IEEE conference on Computer Vision and Pattern Recognition*, pp. 3291-3300, 2018.

[37] Cheng Zhang, Qingsen Yan, Yu Zhu, Xianjun Li, Jinqiu Sun, Yanning Zhang, "Attention-Based Network for Low-Light Image Enhancement," *In: Proceedings of the IEEE International Conference on Multimedia and Expo*, pp.1-6, 2020.

[38] Hansen Feng, Lizhi Wang, Yuzhi Wang and Hua Huang, "Learnability Enhancement for Low-light Raw Denoising: Where Paired Real Data Meets Noise Modeling," *ArXiv abs/2207.06103*, 2022.

[39] Yucheng Lu, and Seung-Won Jung, "Progressive Joint Low-Light Enhancement and Noise Removal for Raw Images," *IEEE Transactions on Image Processing*, vol.31, pp. 2390-2404, 2022.

[40] Xiangyu Xu, Yongrui Ma and Wenxiu Sun, "Towards real scene super-resolution with raw images," *In: Proceedings of the IEEE/CVF Conference on Computer Vision and Pattern Recognition*, pp. 1723-1731, 2019.

[41] Ke Xu, Xin Yang, Baocai Yin, Rynson W.H. Lau, "Learning to restore low-light images via decomposition-and-enhancement," *In: Proceedings of the IEEE/CVF Conference on Computer Vision and Pattern Recognition*, pp. 2281-2290, 2020.

[42] Yufei Wang, Renjie Wan, Wenhan Yang, Haoliang Li, Lap-Pui Chau and Alex Kot, "Low-Light Image Enhancement with Normalizing Flow," *In: Proceedings of the AAAI Conference on Artificial Intelligence*, 2022.

[43] Jiahuan Ren, Zhao Zhang, Jicong Fan, Haijun Zhang, Mingliang Xu and Meng Wang, "Robust Low-rank Deep Feature Recovery in CNNs: Toward Low Information Loss and Fast Convergence," *In: Proceedings of the 21st IEEE International Conference on Data Mining*, Auckland, New Zealand, pp. 529-538, Aug 2021.

[44] Suiyi Zhao, Zhao Zhang, Richang Hong, Mingliang Xu, Haijun Zhang, Meng Wang and Shuicheng Yan, "CRNet: Unsupervised Color Retention Network for Blind Motion Deblurring," *In: Proceedings of the 30th ACM International Conference on Multimedia*, Lisbon, Portugal, June 2022.

[45] R. Feng, C. Li, S. Zhou, W. Sun, Q. Zhu, J. Jiang, Q. Yang, C. C. Loy, and J. Gu, et al., "MIPI 2022 challenge on under-display camera image restoration: Methods and results," *In: Proceedings of the ECCV 2022 Mobile Intelligent Photography and Imaging (MIPI) Workshop*, 2022.

[46] Chongyi Li, Chunle Guo, Linghao Han, Jun Jiang, Ming-Ming Cheng, Jinwei Gu, Chen Change Loy, "Low-Light Image and Video Enhancement Using Deep Learning: A Survey," *IEEE Transactions on Pattern Analysis and Machine Intelligence*, Nov 2021.